The ozone hole indirect effect: Cloud-radiative anomalies accompanying the poleward shift of the eddy-driven jet in the Southern Hemisphere

Kevin M. Grise,[1] Lorenzo M. Polvani,[1,2] George Tselioudis,[2,3] Yutian Wu,[4] and Mark D. Zelinka[5]

Received 7 May 2013; revised 14 June 2013; accepted 16 June 2013.

[1] This study quantifies the response of the clouds and the radiative budget of the Southern Hemisphere (SH) to the poleward shift in the tropospheric circulation induced by the development of the Antarctic ozone hole. Single forcing climate model integrations, in which only stratospheric ozone depletion is specified, indicate that (1) high-level and midlevel clouds closely follow the poleward shift in the SH midlatitude jet and that (2) low-level clouds decrease across most of the Southern Ocean. Similar cloud anomalies are found in satellite observations during periods when the jet is anomalously poleward. The hemispheric annual mean radiation response to the cloud anomalies is calculated to be approximately +0.25 W m^{-2}, arising largely from the reduction of the total cloud fraction at SH midlatitudes during austral summer. While these dynamically induced cloud and radiation anomalies are considerable and are supported by observational evidence, quantitative uncertainties remain from model biases in mean-state cloud-radiative processes. **Citation:** Grise, K. M., L. M. Polvani, G. Tselioudis, Y. Wu, and M. D. Zelinka (2013), The ozone hole indirect effect: Cloud-radiative anomalies accompanying the poleward shift of the eddy-driven jet in the Southern Hemisphere, *Geophys. Res. Lett.*, *40*, doi:10.1002/grl.50675.

1. Introduction

[2] Stratospheric ozone depletion in the late twentieth century is well known to have had a tiny "direct effect" of -0.05 ± 0.10 W m^{-2} on Earth's radiative budget [*Forster et al*., 2007]. At the same time, however, springtime ozone depletion in the Antarctic stratosphere (the "ozone hole") has led to a robust poleward shift in the westerly eddy-driven jet in the Southern Hemisphere (SH) troposphere during late spring and summer (see the recent review by *Thompson et al*. [2011]). As the tropospheric jet shifts poleward, the associated storm track, precipitation, and cloud patterns over the Southern Ocean follow, and the resulting changes in the cloud distribution impact the radiative budget of the SH. The goal of this study is to quantify this "indirect effect" of the ozone-hole-induced tropospheric jet shift.

[3] Recent observations from the International Satellite Cloud Climatology Project (ISCCP) have suggested poleward shifts in the cloud patterns over the midlatitude oceans of both hemispheres, resulting in a positive net radiative effect on the climate system [*Bender et al*., 2012]. However, previous studies have focused on the role of anthropogenic greenhouse gases [*Tselioudis and Rossow*, 2006; *Tsushima et al*., 2006; *Bender et al*., 2012] and have not explored the role of ozone depletion in recent SH cloud changes. Here we examine the impact of Antarctic stratospheric ozone depletion on the clouds and the radiative budget of the SH using a set of carefully designed climate model experiments in which we independently prescribe observed levels of ozone and greenhouse gases during the pre-ozone hole (1960) and ozone hole (2000) periods. Our results demonstrate that during SH summer, ozone depletion leads to a robust change in the cloud distribution over the Southern Ocean and a considerable positive net radiative "indirect effect" on the SH climate system.

2. Methodology

[4] The results in this study are based on climate model experiments with the National Center for Atmospheric Research Community Atmosphere Model version 3 (CAM3) [*Collins et al*., 2006]. The model is integrated with a standard T42 horizontal resolution (~2.8° × 2.8° latitude-longitude grid), 26 hybrid vertical levels, and a model top at 2.2 hPa. The atmospheric model is coupled to a slab ocean model and a thermodynamic sea ice model. Further details of the model configuration are described by *Wu et al*. [2013].

[5] Here, we carry out a set of four 100 year time-slice integrations with fixed seasonally varying forcings. The experiments are nearly identical to those in *Polvani et al*. [2011] (hereafter P11): (1) a control run in which we set ozone and greenhouse gases at 1960 levels (REF1960), (2) a run in which we perturb ozone to 2000 levels (thus creating a springtime ozone hole over Antarctica) and leave greenhouse gases at 1960 levels (OZONE2000), (3) a run in which we perturb greenhouse gases to 2000 levels and leave ozone at 1960 levels (GHG2000), and (4) a run in which we set both ozone and greenhouse gases at 2000 levels (BOTH2000). The ozone levels are taken from *Cionni et al*. [2011], and

[1]Lamont-Doherty Earth Observatory, Columbia University, Palisades, New York, USA.
[2]Department of Applied Physics and Applied Mathematics, and Department of Earth and Environmental Sciences, Columbia University, New York, New York, USA.
[3]NASA Goddard Institute for Space Studies, New York, New York, USA.
[4]Center for Atmosphere Ocean Science, Courant Institute of Mathematical Sciences, New York University, New York, New York, USA.
[5]Program for Climate Model Diagnosis and Intercomparison, Lawrence Livermore National Laboratory, Livermore, California, USA.

Corresponding author: K. M. Grise, Lamont-Doherty Earth Observatory, Columbia University, PO Box 1000, 61 Rt. 9W, Palisades, NY 10964-8000, USA. (kgrise@ldeo.columbia.edu)

0094-8276/13/10.1002/grl.50675

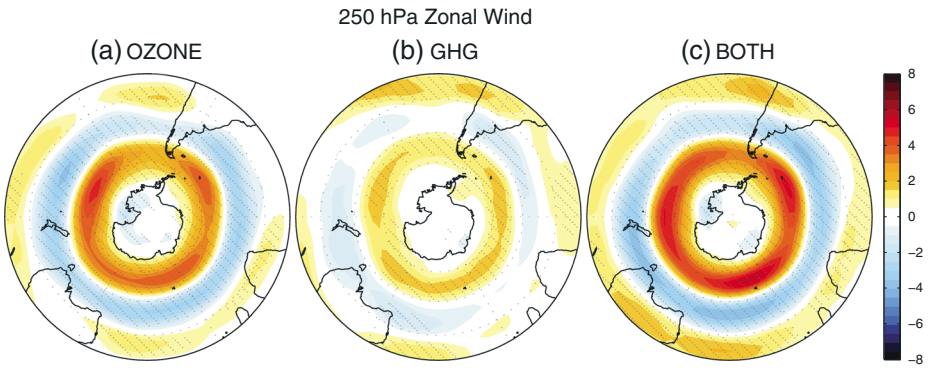

Figure 1. December–February (DJF) 250 hPa zonal wind response to (a) ozone forcing, (b) greenhouse gas forcing, and (c) both forcings. The shading interval is 0.5 m s^{-1}. The stippling indicates regions that are 95% significant via Student's *t* test.

the greenhouse gas levels are taken from Table 1 of P11. The key difference between the experiments discussed in P11 and those analyzed in this paper is that here we use a slab ocean and sea ice model (rather than prescribed sea surface temperatures and sea ice concentrations) to provide an additional degree of realism in the representation of radiative processes in the model. Nonetheless, the major conclusions of this study can be derived using either the slab ocean runs (as shown below) or the prescribed sea surface temperature runs of P11 (see Figure S1 in the supporting information).

[6] In addition to the model experiments, we perform observational analysis using monthly-mean geopotential heights from the European Centre for Medium-Range Weather Forecasts Interim reanalysis data set (ERA-Interim) [*Dee et al*., 2011] and monthly-mean visible/infrared satellite-detected cloud fractions from the ISCCP D2 data set [*Rossow and Schiffer*, 1999]. The ISCCP D2 data are obtained from NASA Goddard Institute for Space Studies on a 2.5° × 2.5° global grid over the period July 1983 to December 2009. To allow for quantitative comparison of the ISCCP and CAM3 cloud variables, we format the CAM3 cloud variables using the ISCCP simulator [*Klein and Jakob*, 1999]. As such, we refer to clouds in three categories based on the apparent cloud top pressure (CTP) of the highest cloud in a vertical column: low clouds (CTP > 680 hPa), middle clouds (440 hPa < CTP < 680 hPa), and high clouds (CTP < 440 hPa).

3. Cloud Response to SH Circulation Changes

[7] Figure 1 shows the responses of the December–February (DJF) 250 hPa zonal wind to the ozone forcing (OZONE2000), greenhouse gas forcing (GHG2000), and both forcings (BOTH2000). Throughout this paper, we use the term *response* to denote the difference of each run from the REF1960 run. As discussed above, stratospheric ozone depletion during SH spring is associated with a substantial poleward shift in the midlatitude jet at tropospheric levels during SH summer (Figure 1a). Increasing greenhouse gases also produce a poleward shift in the SH midlatitude jet, but the magnitude of that poleward jet shift is much weaker than the one associated with the ozone forcing over the 1960–2000 period (Figure 1b). The zonal wind response to both forcings is dominated by the signal from the ozone forcing (Figure 1c). Overall, the results in Figure 1 compare well to those shown in previous studies (e.g., Figure 4 of P11).

[8] The effects of the jet shifts on clouds are illustrated in Figure 2, which shows the responses of the DJF cloud fraction to the ozone forcing, greenhouse gas forcing, and both forcings. The ozone forcing (Figure 2a) leads to an increase in high and middle cloud fractions at high latitudes and in the subtropics and a decrease in high and middle cloud fractions at midlatitudes. Except over Antarctica, the response of the high and middle clouds closely follows the poleward shift of the jet (Figure 1a), the storm tracks, and the attendant changes in precipitation (cf. Figure 12 of P11). In addition, the ozone forcing leads to a decrease in low cloud fraction at high latitudes and a modest increase in low cloud fraction at midlatitudes. The response of the low clouds is not an artifact of our use of the ISCCP simulator; a similar low cloud response can also be derived using the default model cloud variables (Figure S2).

[9] The cloud fraction response to the greenhouse gas forcing (Figure 2b) has similar spatial structure to the response associated with the ozone forcing, but it is weaker in magnitude in the extratropics, consistent with the weaker midlatitude jet shift shown in Figure 1b. Consequently, when both the ozone and greenhouse gas forcings are specified (Figure 2c), the cloud fraction response in the SH extratropics is dominated by the signal from the ozone forcing. Although the greenhouse gas forcing influences clouds in all seasons (not shown), the cloud fraction response to the ozone forcing during DJF is the largest signal in the SH extratropics in our runs.

[10] Given the well-known deficiencies in model representation of clouds, one might rightfully ask: How realistic are the cloud fraction responses shown in Figure 2? Even though CAM3 and CAM4 have been used extensively as part of Phase 3 and the recently completed Phase 5 of the Coupled Model Intercomparison Project, their representation of clouds is plagued by the common "too few, too bright" bias [*Kay et al*., 2012; *Klein et al*., 2013]: Simply stated, the models tend to underestimate total cloud fraction but overestimate cloud optical thickness. Some of these biases have been addressed in the newly released version of CAM (version 5) [*Kay et al*., 2012], but CAM5 is not readily accessible for our experiments at present.

[11] With these caveats in mind, we next compare the cloud fraction anomalies from our CAM3 integrations with observed cloud fraction anomalies from ISCCP. Because observed multidecadal trends in clouds are highly sensitive to inhomogeneities in the satellite-observing system, we examine month-to-month variability in the SH climate system

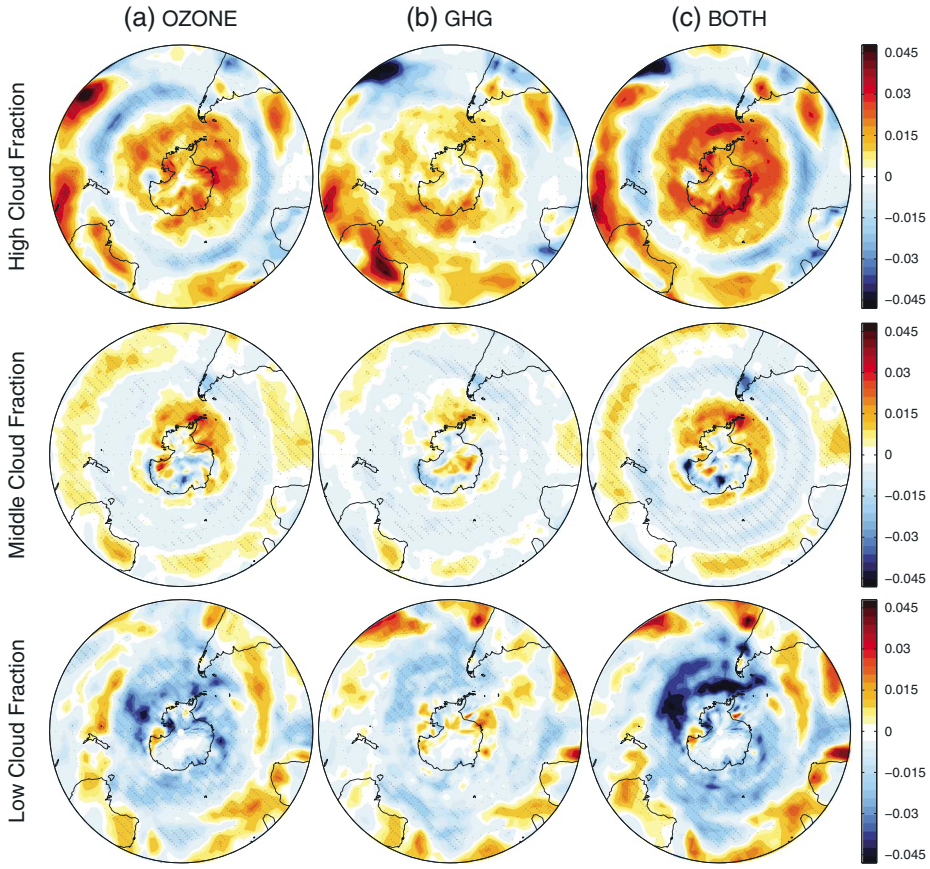

Figure 2. As in Figure 1, but for (top) high cloud fraction, (middle) middle cloud fraction, and (bottom) low cloud fraction. The shading interval is 0.003.

instead of computing trends. The poleward shift in the tropospheric jet associated with Antarctic stratospheric ozone depletion projects very strongly onto the leading mode of internal variability in the SH extratropical circulation, the southern annular mode (SAM) [e.g., *Thompson et al.*, 2011]. Consequently, the cloud signatures associated with the SAM can provide valuable (though qualitative) insight into the cloud signatures associated with the formation of the Antarctic ozone hole.

[12] Figure 3a shows the ISCCP cloud fraction anomalies associated with a +1 standard deviation change in the SAM during DJF, corresponding to a poleward shift in the SH midlatitude jet. To create these plots, we (1) remove the seasonal cycle and long-term trend from monthly-mean DJF data over the period December 1983 to December 2009, (2) calculate the leading principal component (PC) time series of ERA-Interim 500 hPa geopotential height anomalies over the domain 20°S-90°S, and (3) regress the ISCCP cloud fraction anomalies onto the standardized PC time series. The observations clearly indicate that an anomalously poleward midlatitude jet in the SH is associated with an increase in high cloud fraction over the high-latitude Southern Ocean, a decrease in low cloud fraction over the high-latitude Southern Ocean, and an increase in low cloud fraction at midlatitudes.

[13] For a direct comparison with observations, we also show the cloud fraction anomalies associated with +1 standard deviation change in the model SAM during DJF (Figure 3b). Here the SAM is calculated as above, but using the 500 hPa geopotential height field from the BOTH2000 model integration, the best analog to the observational period. The model cloud fraction anomalies associated with the SAM have strong resemblance to both (1) the observed cloud fraction anomalies associated with the SAM (Figure 3a) and (2) the model cloud fraction response to the ozone forcing (Figure 2a). Discrepancies between the ISCCP and CAM3 results are most notable in the middle cloud fraction field and over Antarctica, where the accuracy of the clouds in both ISCCP and CAM3 is likely the most questionable. Despite these limitations, CAM3 appears to provide a reasonable representation of the cloud fraction anomalies associated with a poleward shifted jet in the SH troposphere.

4. Cloud-Radiative Anomalies Accompanying the SH Tropospheric Jet Shift

[14] The results of the previous section clearly indicate that Antarctic stratospheric ozone depletion has not only played an appreciable role in recent SH tropospheric circulation trends but is also linked to systematic changes in the SH cloud field. Using our model output, we now estimate the net "indirect effect" of these ozone hole-induced cloud anomalies on the radiative budget of the SH. To do this, we multiply the cloud fraction response to the ozone forcing (Figure 2a) by the cloud radiative kernels of *Zelinka et al.* [2012] and then sum over all cloud types. The kernels quantify the perturbation in net downward top-of-atmosphere radiation associated with a given cloud fraction change, but are not biased by changes

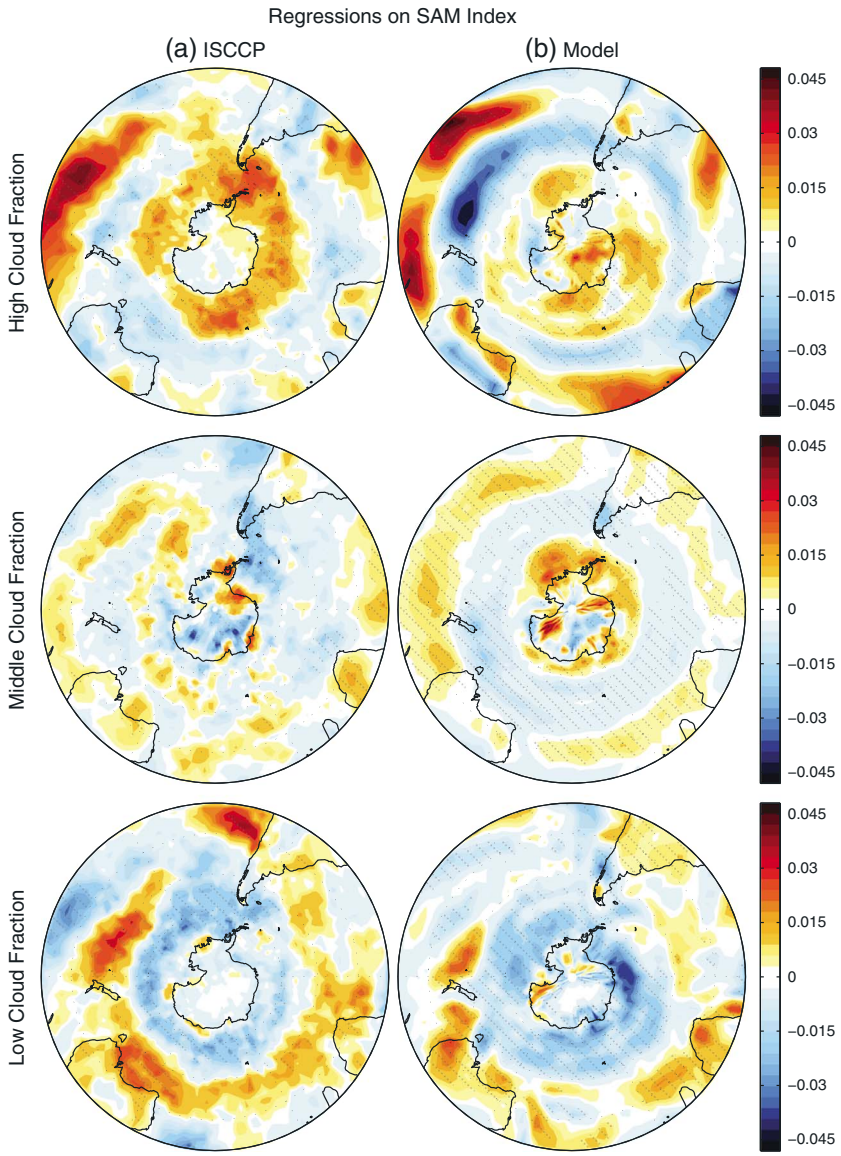

Figure 3. Regressions of monthly-mean DJF cloud fraction anomalies on the SAM index for (a) ISCCP observations (December 1983 to December 2009) and (b) the BOTH2000 model integration. The shading interval is 0.003. Units are per standard deviation in the SAM index. The stippling indicates regions that are 95% significant via Student's *t* test.

in temperature, water vapor, or surface albedo (as are the cloud-radiative effects directly output from the model).

[15] Figure 4 shows the kernel estimates of the cloud-induced radiation anomalies associated with the ozone forcing. The longwave radiation anomalies (Figure 4a) are caused primarily by changes in high cloud fraction and have a hemispheric-mean value of $+0.11 \pm 0.08$ W m^{-2} (90% confidence range) in DJF, and $+0.07 \pm 0.06$ W m^{-2} in the annual mean. The shortwave radiation anomalies (Figure 4b) are caused primarily by changes in total cloud fraction and have a hemispheric-mean value of $+0.25 \pm 0.16$ W m^{-2} in DJF, and $+0.18 \pm 0.07$ W m^{-2} in the annual mean. The total radiation anomalies are dominated by the positive shortwave contribution from midlatitudes (Figure 4c), yielding a net hemispheric-mean warming "indirect effect" of $+0.36 \pm 0.13$ W m^{-2} in DJF and $+0.25 \pm 0.05$ W m^{-2} in the annual mean. Similar results can be derived using the cloud-radiative effects directly output from CAM3 (Figure S3). Note also that during SH summer, the cloud-induced radiation anomalies associated with the ozone forcing are larger than those associated with increasing greenhouse gases over the 1960–2000 period (Figure S4).

[16] Figure 4 provides the first order-of-magnitude estimate of the "indirect effect" of the ozone hole on the SH radiative budget, but we caution that the net value of this effect may be difficult to determine accurately. First, while our model experiments provide a reasonable representation of the cloud anomalies associated with a poleward shifted SH midlatitude jet, the results are only derived from one model with known deficiencies in its mean-state representation of clouds and shortwave cloud-radiative effects in the SH extratropics [*Kay et al.*, 2012]. Second, the hemispheric-mean values of the cloud-induced radiation anomalies reflect the residuals of large opposing contributions at high, middle, and low latitudes (Figure 4c). Subtle differences between the model cloud responses to the ozone forcing (Figure 2a) and the SAM (Figure 3b) have a nonnegligible impact on the magnitude of

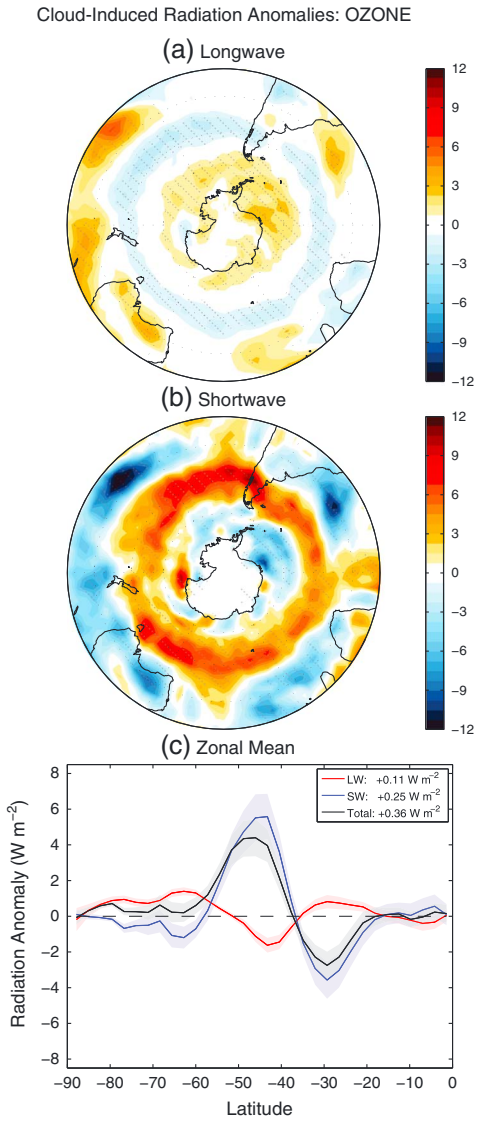

Figure 4. DJF cloud-induced top-of-atmosphere radiation anomalies (as defined by the radiative kernels of *Zelinka et al*. [2012]) associated with the ozone forcing: (a) longwave (LW) contribution, (b) shortwave (SW) contribution, and (c) zonal mean of LW, SW, and total radiation anomalies. The shading interval in Figures 4a and 4b is 0.75 W m^{-2}. The stippling in Figures 4a and 4b indicates values that are 95% significant; the shaded error bounds in Figure 4c indicate 95% confidence intervals. Values averaged over the SH are listed in the legend of Figure 4c. Annual-mean, hemispheric-mean values are +0.07 W m^{-2} (LW), +0.18 W m^{-2} (SW), and +0.25 W m^{-2} (total).

the hemispheric-mean radiation values (compare Figure 4 with Figure S5). Thus, it is possible that an underestimate of the low cloud response at SH mid-latitudes by the model (compare bottom row of Figure 3) could reverse the sign of the "indirect effect".

[17] Finally, we note that the large positive shortwave radiation anomaly at SH midlatitudes induced by the ozone hole could contribute to shifting the latitude of the maximum meridional surface temperature gradient and eddy-driven jet over the Southern Ocean [see also *Ceppi et al*., 2012]. Future work is needed to understand the linkages among stratospheric ozone depletion, tropospheric circulation shifts, cloud changes, and radiative anomalies in the SH.

[18] **Acknowledgments.** We thank two anonymous reviewers for their helpful comments and G. J. P. Correa for assistance with the model experiments. K.M.G. and L.M.P. were supported by a National Science Foundation grant to Columbia University. M.D.Z.'s contribution was performed under the auspices of U.S. Department of Energy (DOE) by Lawrence Livermore National Laboratory under contract DE-AC52-07NA27344 and was supported by the Regional and Global Climate and Earth System Modeling programs of the U.S. DOE's Office of Science.

[19] The Editor thanks two anonymous reviewers for their assistance in evaluating this paper.

References

Bender, F. A.-M., et al. (2012), Changes in extratropical storm track cloudiness 1983–2008: Observational support for a poleward shift, *Clim. Dyn.*, *38*, 2037–2053.

Ceppi, P., et al. (2012), Southern Hemisphere jet latitude biases in CMIP5 models linked to shortwave cloud forcing, *Geophys. Res. Lett.*, *39*, L19708, doi:10.1029/2012GL053115.

Cionni, I., et al. (2011), Ozone database in support of CMIP5 simulations: Results and corresponding radiative forcing, *Atmos. Chem. Phys.*, *11*, 11,267–11,292.

Collins, W. D., et al. (2006), The formulation and atmospheric simulation of CAM3, *J. Clim.*, *19*, 2144–2161.

Dee, D. P., et al. (2011), The ERA-Interim reanalysis: Configuration and performance of the data assimilation system, *Q. J. R. Meteorol. Soc.*, *137*, 553–597.

Forster, P., et al. (2007), Changes in atmospheric constituents and in radiative forcing, in *IPCC Climate Change 2007: The Physical Science Basis*, edited by S. Solomon et al., pp. 129–234, Cambridge Univ. Press, Cambridge, U. K.

Kay, J., et al. (2012), Exposing global cloud biases in CAM using satellite observations and their corresponding instrument simulators, *J. Clim.*, *25*, 5190–5207.

Klein, S. A., and C. Jakob (1999), Validation and sensitivities of frontal clouds simulated by the ECMWF model, *Mon. Weather Rev.*, *127*, 2514–2531.

Klein, S. A., et al. (2013), Are climate model simulations of clouds improving? An evaluation using the ISCCP simulator, *J. Geophys. Res. Atmos.*, *118*, 1329–1342, doi:10.1002/jgrd.50141.

Polvani, L. M., et al. (2011), Stratospheric ozone depletion: The main driver of twentieth century atmospheric circulation changes in the Southern Hemisphere, *J. Clim.*, *24*, 795–812.

Rossow, W. B., and R. A. Schiffer (1999), Advances in understanding clouds from ISCCP, *Bull. Am. Meteorol. Soc.*, *80*, 2261–2287.

Thompson, D. W. J., et al. (2011), Signatures of the Antarctic ozone hole in Southern Hemisphere surface climate change, *Nat. Geosci.*, *4*, 741–749.

Tselioudis, G., and W. B. Rossow (2006), Climate feedback implied by observed radiation and precipitation changes with midlatitude storm strength and frequency, *Geophys. Res. Lett.*, *33*, L02704, doi:10.1029/2005GL024513.

Tsushima, Y., et al. (2006), Importance of the mixed-phase cloud distribution in the control climate for assessing the response of clouds to carbon dioxide increase: A multi-model study, *Clim. Dyn.*, *27*, 113–126.

Wu, Y., et al. (2013), The importance of the Montreal Protocol in protecting Earth's hydroclimate, *J. Clim.*, *26*, 4049–4068, doi:10.1175/JCLI-D-12-00675.1.

Zelinka, M. D., et al. (2012), Computing and partitioning cloud feedbacks using cloud property histograms. Part I: Cloud radiative kernels, *J. Clim.*, *25*, 3715–3735.

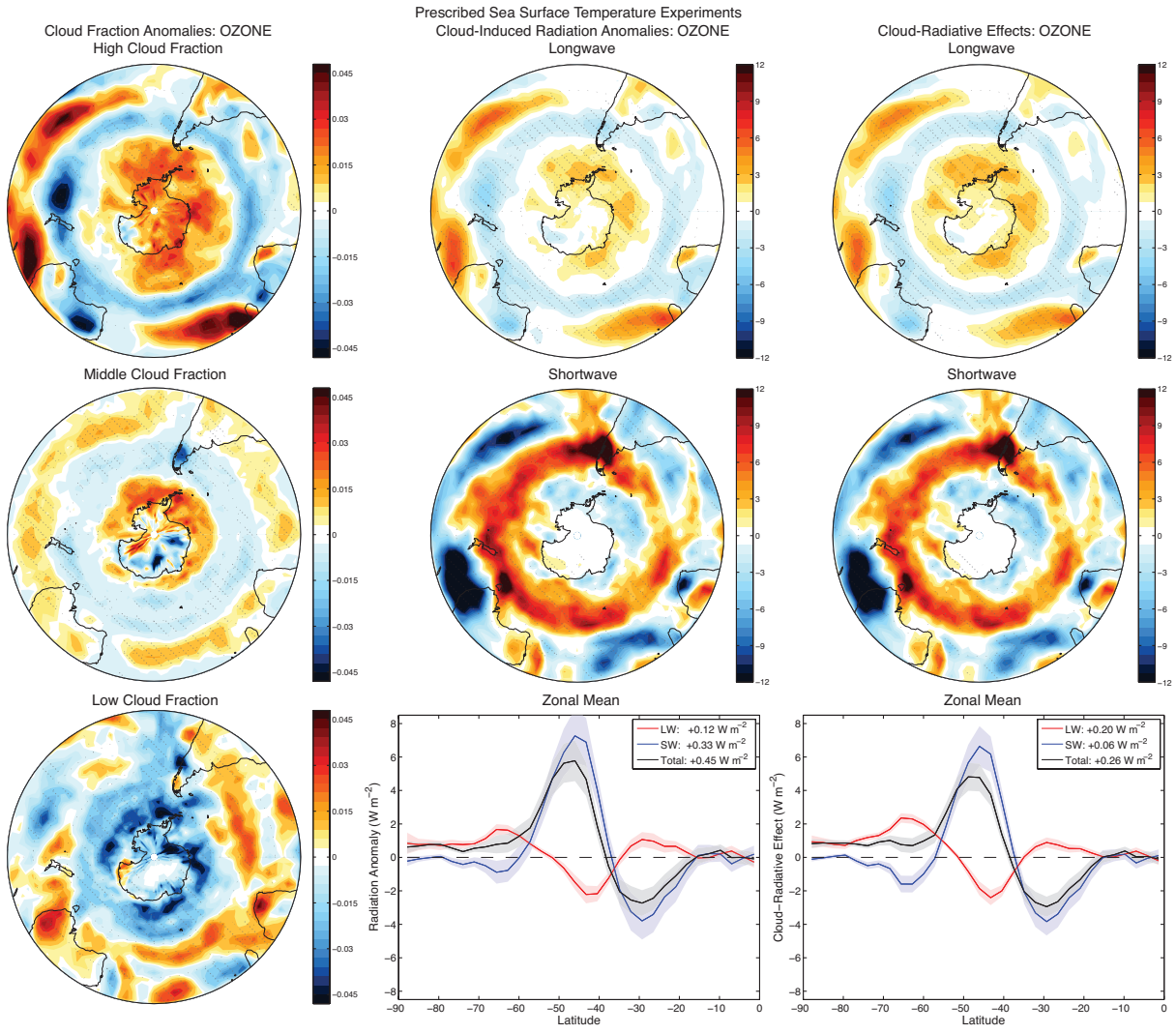

Figure S1. (Left column) As in the left column of Fig. 2, but for the prescribed sea surface temperature model experiments of *Polvani et al.* [2011]. (Middle column) As in Fig. 4, but for the prescribed sea surface temperature model experiments of *Polvani et al.* [2011]. Values averaged over the Southern Hemisphere are listed in the legend of the bottom panel. Annual-mean values are +0.13 W m^{-2} (LW), +0.16 W m^{-2} (SW), and +0.29 W m^{-2} (total). Annual-mean, global-mean values are +0.10 W m^{-2} (LW), +0.12 W m^{-2} (SW), and +0.22 W m^{-2} (total). (Right column) As in the middle column, but for the DJF cloud-radiative effects directly output from the model. Annual-mean values are +0.16 W m^{-2} (LW), +0.03 W m^{-2} (SW), and +0.19 W m^{-2} (total). Annual-mean, global-mean values are +0.12 W m^{-2} (LW), 0 W m^{-2} (SW), and +0.12 W m^{-2} (total). [The annual-mean, global-mean top-of-atmosphere clear-sky radiative response to the ozone forcing is +0.04 W m^{-2} (LW), -0.21 W m^{-2} (SW), and -0.17 W m^{-2} (total); the annual-mean, global-mean top-of-atmosphere all-sky radiative response to the ozone forcing is +0.16 W m^{-2} (LW), -0.21 W m^{-2} (SW), and -0.05 W m^{-2} (total).]

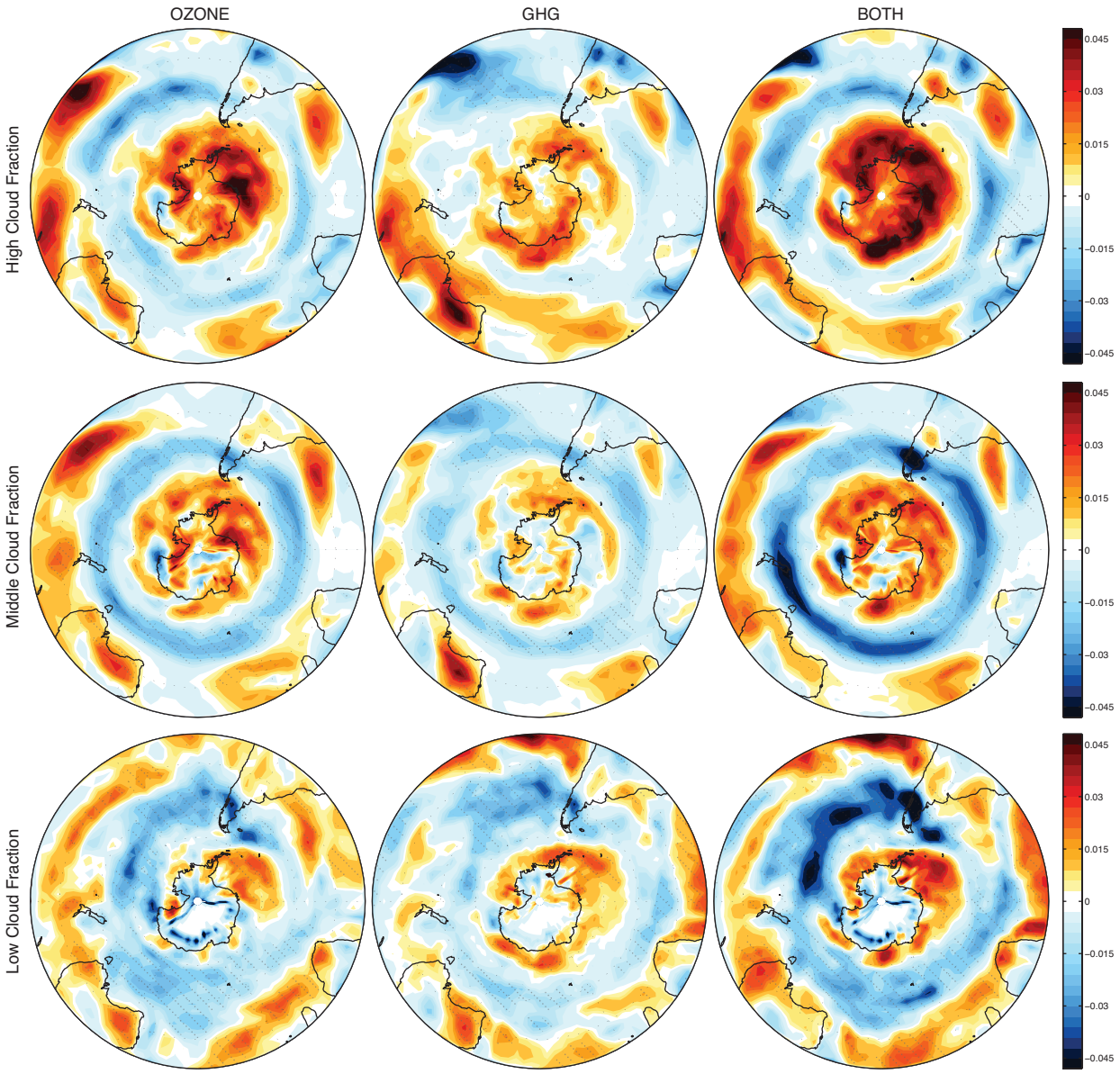

Figure S2. As in Fig. 2, but for the default model cloud variables not calculated using the ISCCP simulator.

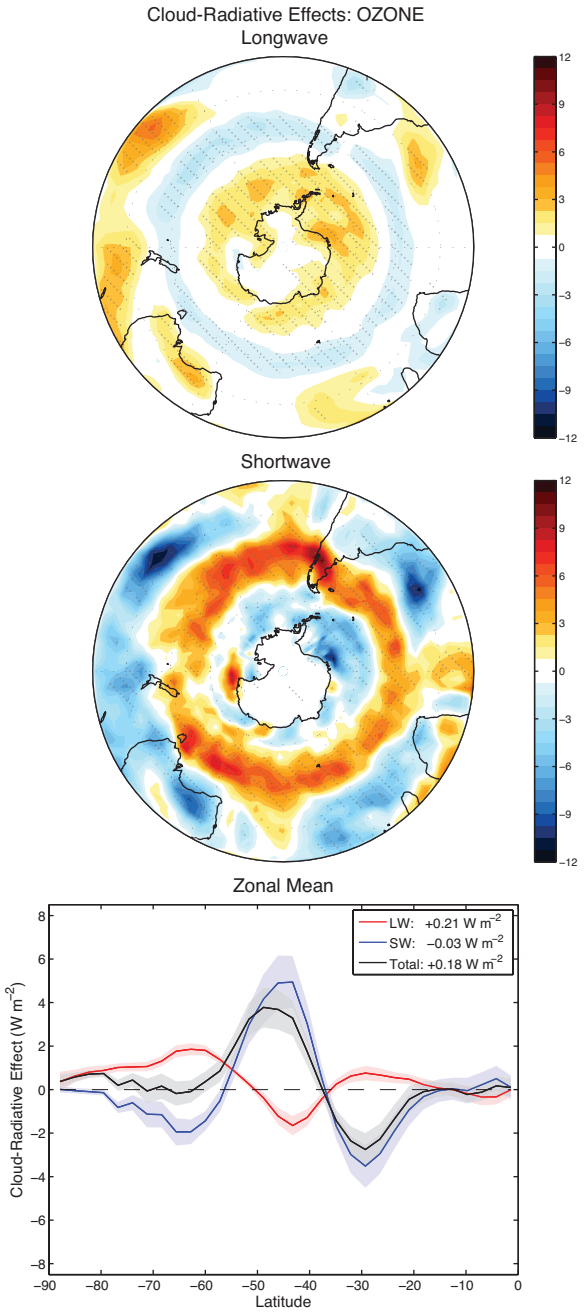

Figure S3. As in Fig. 4, but for the DJF cloud-radiative effects directly output from the model. Annual-mean, hemispheric-mean values are +0.14 W m^{-2} (LW), +0.01 W m^{-2} (SW), and +0.15 W m^{-2} (total).

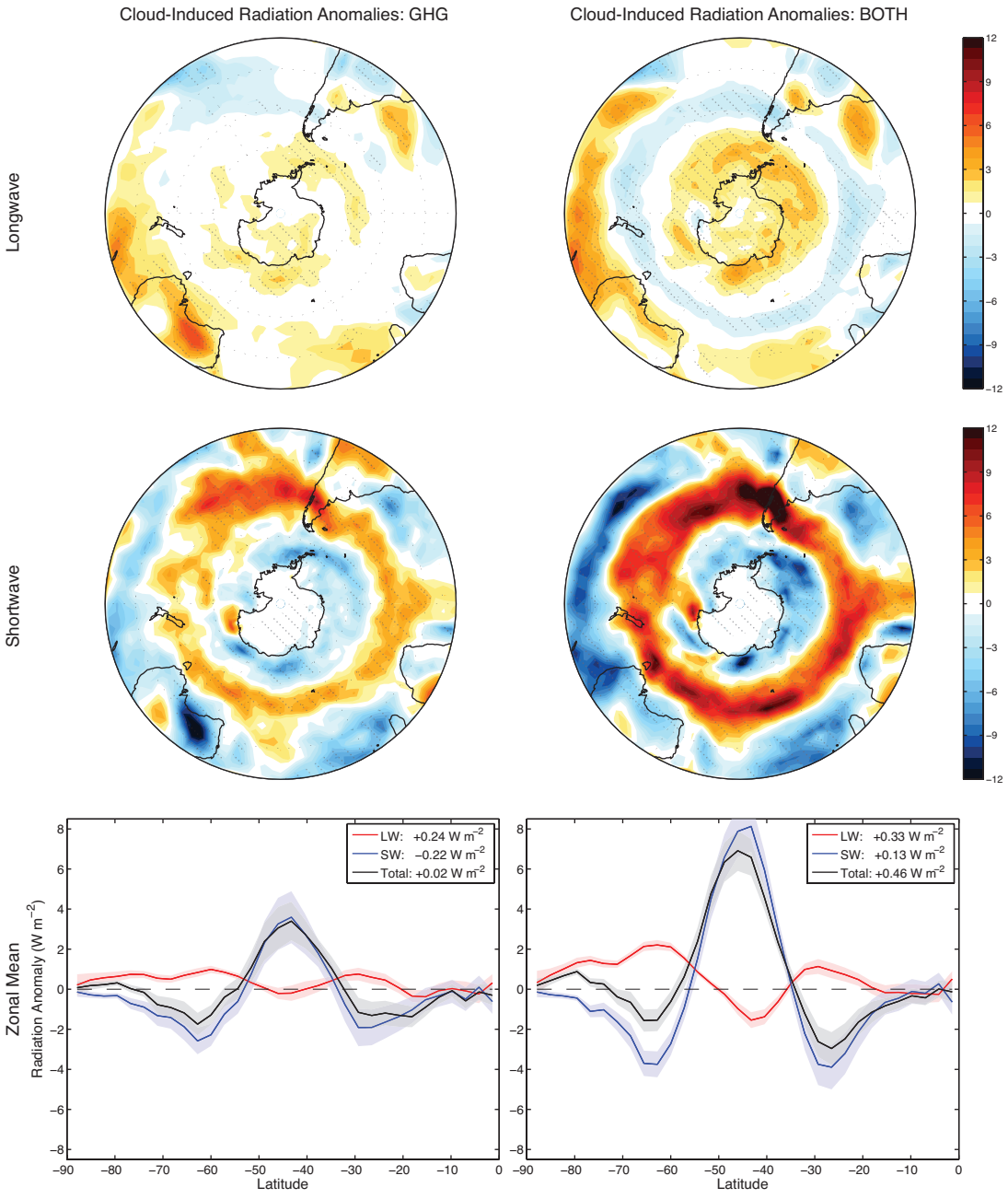

Figure S4. As in Fig. 4, but for the DJF cloud-induced top-of-atmosphere radiation anomalies associated with (left column) the greenhouse gas forcing and (right column) both the ozone and greenhouse gas forcings. For the greenhouse gas forcing, the annual-mean, hemispheric-mean values are +0.24 W m^{-2} (LW), -0.13 W m^{-2} (SW), and +0.11 W m^{-2} (total). For both forcings, the annual-mean, hemispheric-mean values are +0.43 W m^{-2} (LW), -0.06 W m^{-2} (SW), and +0.37 W m^{-2} (total).

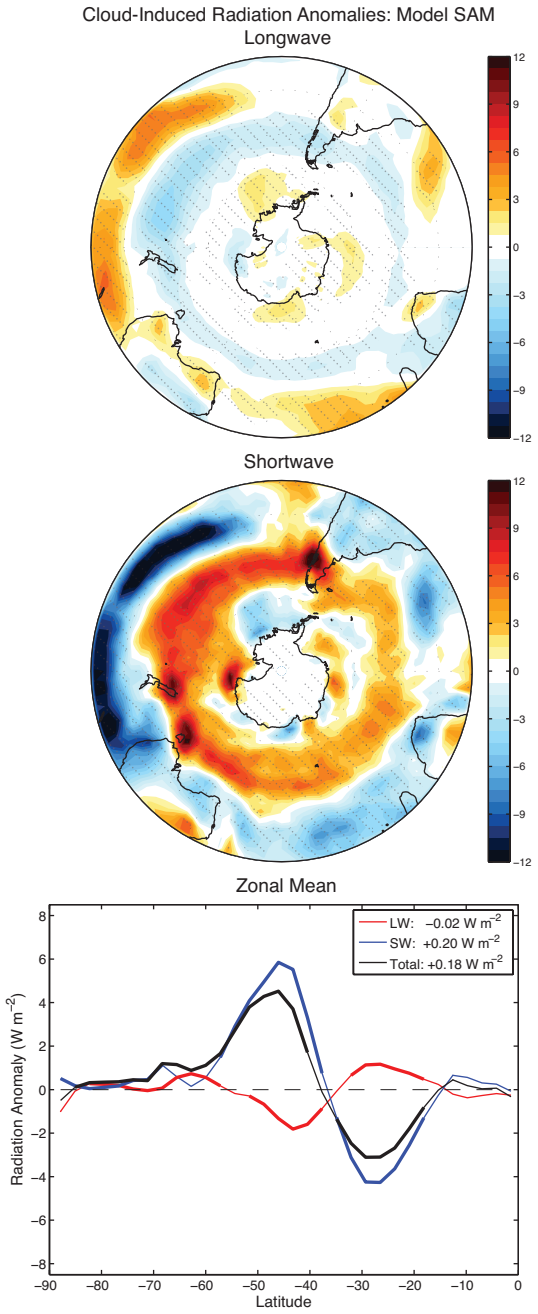

Figure S5. As in Fig. 4, but for the monthly cloud-induced radiation anomalies associated with a +1 standard deviation fluctuation in the model SAM (i.e., the radiation anomalies corresponding to the cloud pattern in Fig. 3b). The stippling in the top two panels and bolded lines in the bottom panel indicate values that are 95% significant via a Student's *t*-test.